tvst

Article

Association Between the Types of Posterior Staphyloma and Their Risk Factors in Pathological Myopia

Guangqi An[1–3,*], Fangfang Dai[1,*], Rui Wang[1,3], Zhenhui Liu[2,3], Ju Guo[2,3], Meng Pan[2,3], Xuemin Jin[1–3], and Bo Lei[1,3]

[1] Zhengzhou University People's Hospital, Henan Eye Hospital and Henan Eye Institute, Henan Provincial People's Hospital, Zhengzhou, Henan, China
[2] The First Affiliated Hospital of Zhengzhou University, Zhengzhou, Henan, China
[3] Academy of Medical Sciences of Zhengzhou University, Zhengzhou, Henan, China

Correspondence: Bo Lei, Zhengzhou University People's Hospital, Henan Eye Hospital and Henan Eye Institute, Academy of Medical Sciences of Zhengzhou University, Henan Provincial People's Hospital, Zhengzhou, Henan 450003, China.
e-mail: bolei99@126.com
Xuemin Jin, The First Affiliated Hospital of Zhengzhou University, Academy of Medical Sciences of Zhengzhou University, Zhengzhou, Henan, 450052, China.
e-mail: jinxuemin@zzu.edu.cn

Received: September 8, 2020
Accepted: February 23, 2021
Published: April 8, 2021

Keywords: pathologic myopia; posterior staphyloma; myopic retinoschisis; age; three-dimensional magnetic resonance imaging (3D-MRI)

Citation: An G, Dai F, Wang R, Liu Z, Guo J, Pan M, Jin X, Lei B. Association between the types of posterior staphyloma and their risk factors in pathological myopia. Trans Vis Sci Tech. 2021;10(4):5, https://doi.org/10.1167/tvst.10.4.5

Purpose: The purpose of this study was to investigate the relationship of posterior staphyloma (PS) types in pathological myopia (PM) with age, best-corrected visual acuity (BCVA), spherical equivalent (SE), axial length (AL), and myopic retinoschisis (MRS) using three-dimensional magnetic resonance imaging (3D-MRI) and optical coherence tomography (OCT).

Methods: This retrospective, cross-sectional study included 108 eyes of 59 patients with PM from the Henan Eye Institute, China. We classified the PS types based on current international classification criteria and analyzed the risk factors (age, AL, MRS, and BCVA).

Results: Most of the patients with bilateral PM had the same PS type (80.43%) in both eyes. Complex PS was more common in elderly patients than in younger patients ($P < 0.05$). Eyes with wide macular PS had a longer AL ($P = 0.012$) and worse BCVA ($P = 0.049$) than those with other PS types. MRS was always comorbid with PS (93.33%), and macular PS was the most common (82.14%).

Conclusions: Complex PS is associated with patient age. PS is related to MRS, and these changes observed by 3D-MRI and OCT affect the prognosis of visual acuity. The 3D-MRI scans shows changes in the eye shape and PS efficiently.

Translational Relevance: In patients with PM, 3D-MRI can guide the planning of posterior scleral reinforcement.

Introduction

The incidence of myopia has recently increased, particularly in East Asian countries, including China,[1–3] Japan,[4] and Korea.[5] The prevalence of pathologic myopia (PM) has risen with the increase in myopia cases.[6] PM is usually binocular, and patients tend to be relatively young. PM is an essential factor affecting social and economic development.[7] Although extensive research on myopia, high myopia, and PM has been conducted, measures to prevent the progression of myopia remain limited.[8] Therefore, understanding the pathological changes caused by PM and its related risk factors is extremely important.

Copyright 2021 The Authors

This work is licensed under a Creative Commons Attribution-NonCommercial-NoDerivatives 4.0 International License.

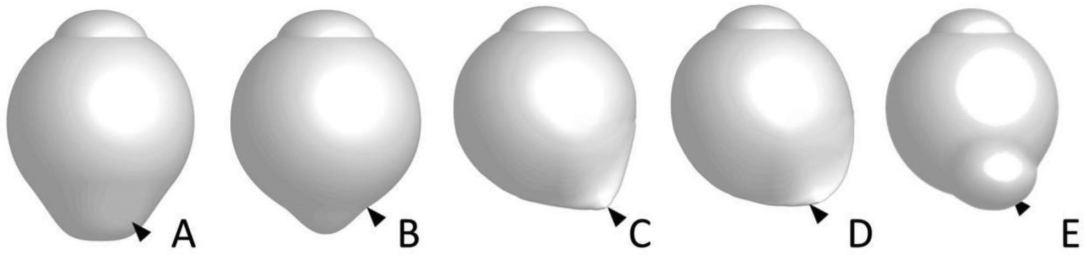

Figure 1. Ohno-Matsui's classification of PS, the norma basilaris of the right eye. Wide macular staphyloma (**A**): wide protrusion behind the eyeball; the protrusion is wide and blunt. Narrow macular staphyloma (**B**): narrow protrusion behind the eyeball; the protrusion is pyramidal. Peripapillary staphyloma (**C**): limited protrusions around the attachment point of the optic nerve; the change in curvature to the protrusion is relatively linear. Nasal staphyloma (**D**): a protrusion on the nasal side of the eye, with a wider area and a smoother curvature. Inferior staphyloma (**E**): a large protrusion on the lower segment of the eyeball; the curvature under the protrusion is not obvious (drawn by Guangqi An).

PM is defined as "excessive axial elongation associated with myopia that leads to structural changes in the posterior segment of the eye (including posterior staphyloma [PS], myopic macular degeneration, myopic traction maculopathy, and high myopia-associated optic neuropathy) and that can lead to loss of best-corrected visual acuity."[9,10] PS is the most destructive pathological feature of PM.[11] With the development of imaging technologies, researchers have succeeded in using three-dimensional magnetic resonance imaging (3D-MRI) to revise the PS classification, which was previously diagnosed by ophthalmoscopy. The 3D-MRI can be used to evaluate the eye shape in PM, PS and best-corrected visual acuity (BCVA).[12,13] PS is the main factor of myopic maculopathy, which plays an essential role in irreversible visual impairment due to PM.[14,15]

This study was conducted in Asian patients with PM in Henan Province, China. We used 3D-MRI to investigate the relationship among the PS type and age, BCVA, spherical equivalent (SE), and axial length (AL). We discussed the alterations in the eye shape and PS with age in PM eyes and the differences in AL, SE, and BCVA in different types of PS to guide the surgical approach.

Materials and Methods

The study participants were patients who visited the Henan Eye Institute from February 2017 to November 2019 and had a clinical diagnosis of PM. The inclusion criteria were as follows: SE < -8.0 diopters (D) or AL >26.5 mm. The exclusion criteria were as follows: (1) serious systemic diseases unsuitable for 3D-MRI testing or poor-quality 3D-MRI scans; (2) glaucoma, diabetic retinopathy, or uveitis; or (3) previous eye surgery or an ocular trauma history affecting the eye structure. Based on the Declaration of Helsinki, we collected demographic information and clinical examination results after informed consent was obtained from the patients. The clinical examination results included BCVA, SE, AL, and fundus photographs, as well as optical coherence tomography (OCT) and 3D-MRI scans.

The patients in this study had undergone 3D-MRI examination at their first visit to the clinic or before posterior scleral reinforcement (PSR) surgery. The 3D-MRI scanning method was described in our previous study,[16] and was performed by skilled radiologists. The patients were scanned using MRI (Siemens Prism 3.0T, Germany, or GE Discovery 750 plus 3.0T, America) and 32-channel head coils to generate a 3D sequence for 3.0 minutes and 18 seconds. The scan range covered the entire head. A sagittal cube imaging technique (cube) was used. The parameters were as follows: repetition time (TR) = 2000.0 ms; echo time (TE) = approximately 110.0 to 120.0 ms; section thickness = 1.0 mm with a 0-mm section gap, number of layers = 128; echo train length = 90; and field of vision = 256 × 230 mm. Volume rendering of the image was generated by high-resolution 3D data from a computer workstation (ADW version 4.6 post-processing workstation). According to the eye shape types proposed by Moriyama et al.[17] and Guo et al.,[12] we analyzed the patients' eye shapes. PS was defined on 3D-MRI images according to Spaide,[18] as follows: "An outpouching of a circumscribed posterior fundus region and has a curvature radius that is smaller than the curvature radius of the adjacent eyewall." According to Curtin's classification,[11] we divided PS into simple staphyloma (types I to V) and

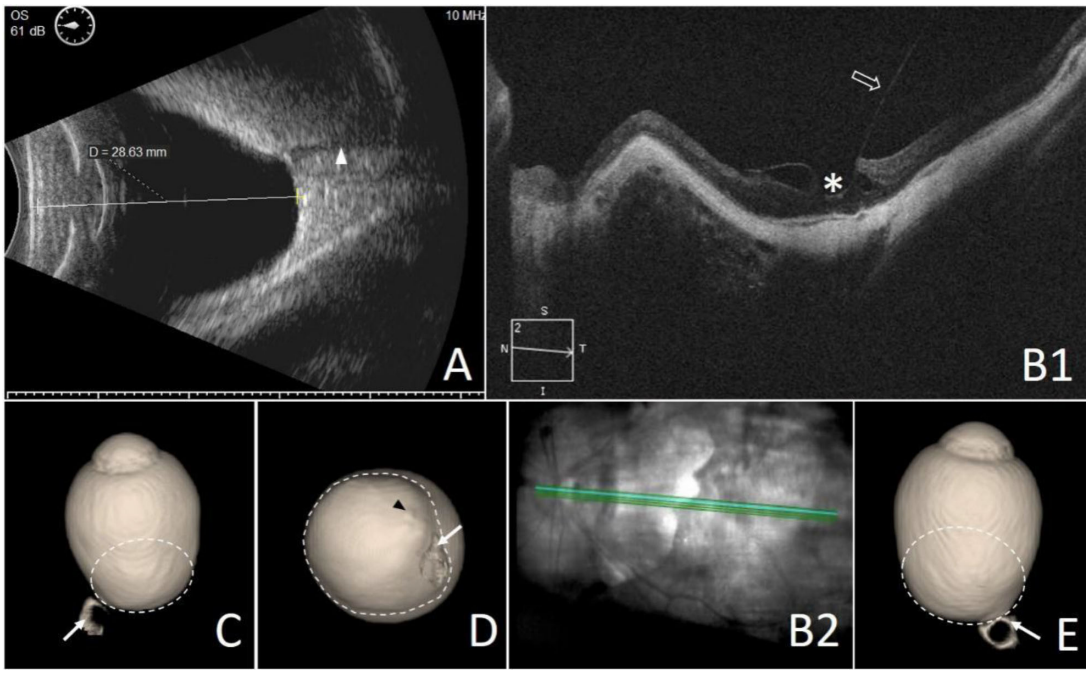

Figure 2. Binocular barrel-shaped eyes with wide macular staphylomas. Binocular PM in a 73-year-old female patient whose SEs were −16 D/−19 D, BCVA values were 0.70 Log MAR/1.00 Log MAR, and ALs were 30.52 mm/31.06 mm in the right and left eyes, respectively. The *white arrow* in the figure shows the optic nerve. B-Us of the left eye (**A**): the *white triangle* indicates the optic nerve, and the posterior of the eyeball is *rectangular*. OCT of the left eye (B1, B2): the *white hollow arrow* indicates vitreous traction, and the *asterisk* indicates an inner macular hole; the choroid is extremely thin, and a large area of atrophy is shown by the infrared fundus image. A 3D-MRI of the left eye (C, D): the norma basilaris and norma occipitalis; the temporal side of the eyeball is symmetrical and, cylindrical, and the *white dashed line* indicates the PS. The PS is wide and large, indicating wide macular PS. The *black arrow* shows an irregular protuberance in the PS. A 3D-MRI of the right eye (**E**): the norma basilaris; the eyeball is cylindrical with wide macular PS, the same as in the left eye.

complex staphyloma (types VI to X). A simple staphyloma is a region with only one radius of curvature. A complex staphyloma is an expansion that has two distinct radii of curvature with a total or partial overlap in the curves. According to Ohno-Matsui's classification[13] of PS, we divided PS into type I (wide, macular staphyloma), type II (narrow, macular staphyloma), type III (peripapillary staphyloma), type IV (nasal staphyloma), type V (inferior staphyloma), and others (staphylomas other than types I to V; Fig. 1). The 3D-MRI scans were independently typed by two experienced ophthalmologists (Liu and Pan) and decided by a third senior ophthalmologist (Jin) in cases of disagreement.

Skilled ophthalmologists performed OCT (Carl Zeiss Meditec Inc.; SW version 4.5.1.11, Germany), which included single and multiline scanning and horizontal, vertical, and inclined multimode scanning with a scan line length approximately 6 to 9 mm, to determine the presence of fundus lesions on the images. They focused on MRS images. The results of OCT were interpreted by two experienced ophthalmologists (Wang and Guo) and were finally approved by a senior doctor (Dai). According to the morphology of MRS, Wang, Guo, and Dai divided MRS into inner retinoschisis (nerve fiber layer and ganglion cell layer), outer retinoschisis (outer plexiform layer and outer nuclear layer), and mixed retinoschisis (inner + outer retinoschisis).[15,19]

Experienced optometrists tested the BCVA and SE. AL was measured using an IOL-Master (Carl Zeiss; IOL-Master (R) Advanced Technology version 5.4, Germany). Fundus photographs were taken using a 45 degree fundus camera (Carl Zeiss; VISUCAM 224, Germany) or a wide-field fundus camera (Optos PLC; Optomap plus, Scotland).

We used SPSS statistics 25.0 software (IBM Corp.) for all data analyses. The χ^2 test was used to analyze the categorical data, which are described using frequencies and percentages. Correlations are expressed using Cramer's V coefficients. The Kolmogorov-Smirnov test was performed to verify whether all the data sets were distributed normally. Normally distributed continuous data are described by the mean and standard deviation, and ANOVA was used for comparisons. A P value <0.05 was considered statistically significant.

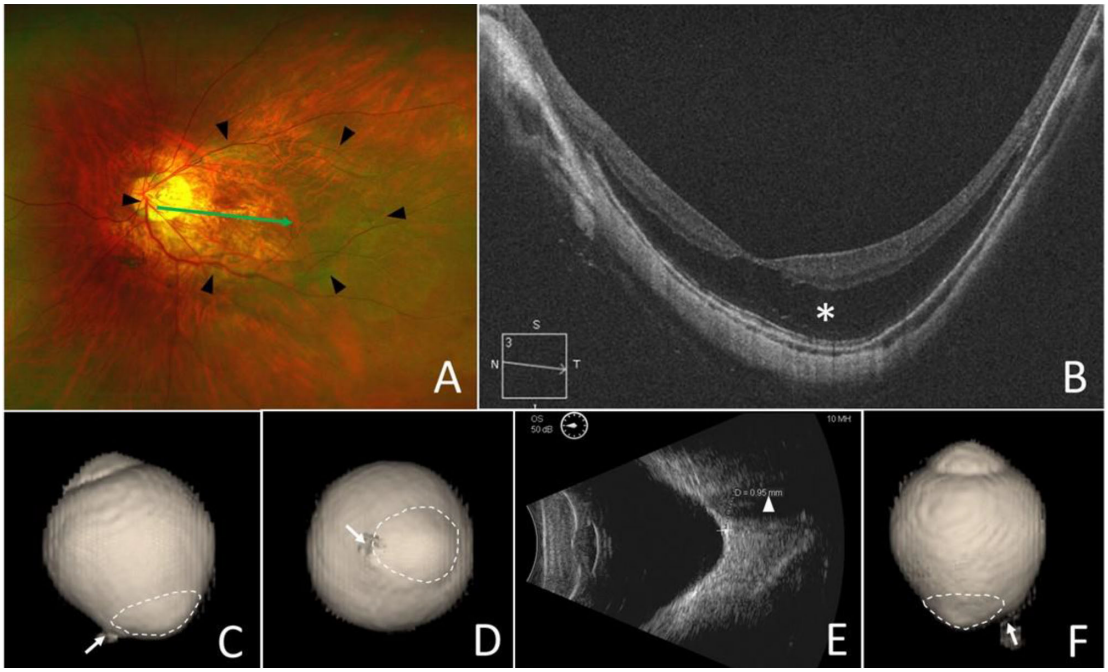

Figure 3. Binocular conical-shaped eyes with narrow macular staphylomas. Binocular PM in a 47-year-old female patient whose SEs were −14 D/−13 D, BCVA values were 0.82 LogMAR/0.30 LogMAR, and ALs were 30.16 mm/30.08 mm in the right and left eyes, respectively. The *white arrow* in the figure indicates the optic nerve. Fundus photograph and OCT of the left eye (**A**, **B**): the *green arrow* indicates the OCT scanning line. The *black arrow* indicates PS confined to the macular area, and the outer retina has retinoschisis formed at the PS area, indicated by the *asterisk*. The 3D-MRI of the left eye (**C**, **D**): the norma basilaris and norma occipitalis; the temporal and nasal sides of the eyeball are symmetrical and conical, and the *white dashed line* indicates the PS. The PS is more limited, indicating narrow macular PS, which is conical. B-Us of the left eye **B**: the *white triangle* indicates the optic nerve, and the posterior of the eyeball is conical. The 3D-MRI of the right eye (**F**): the norma basilaris; the eye shape is conical, and the PS is of the narrow macular type, consistent with the left eye.

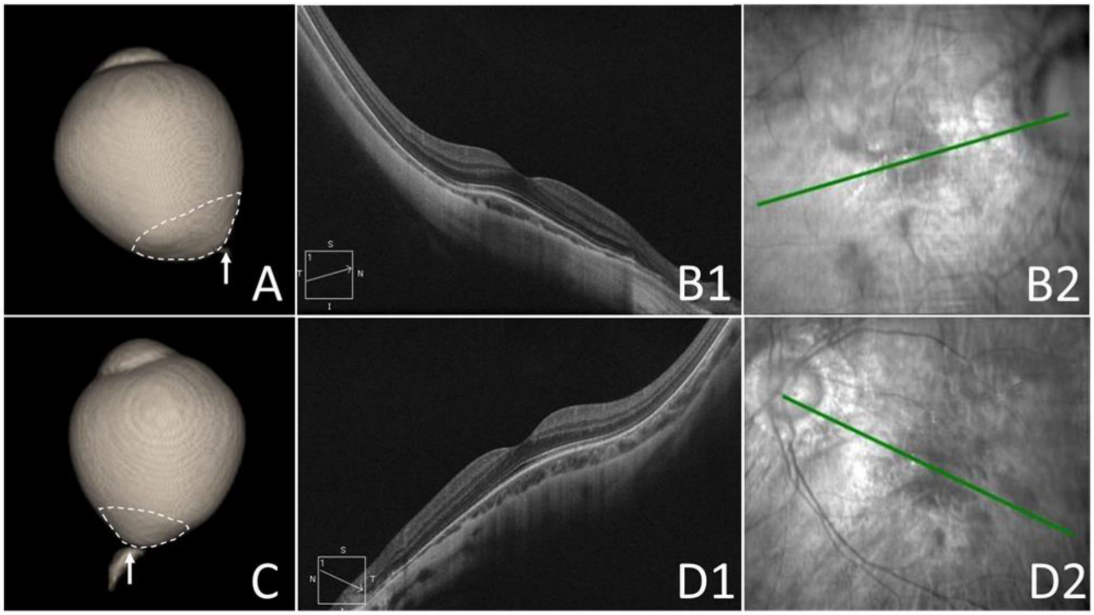

Figure 4. Binocular nasally distorted shaped eyes, peripapillary staphylomas. Binocular PM in a 22-year-old female patient whose SEs were −20 D/−18 D, BCVA values were 0.70 Log MAR/0.40 Log MAR, and ALs were 30.19 mm/29.14 mm in the right and left eyes, respectively. The white arrow in the figure indicates the optic nerve. 3D-MRI and OCT of the right eye (A, B1, B2): the norma basilaris; the white dashed line indicates the area of PS, the top of which is the point of optic nerve attachment. OCT shows the macula located on a slope. 3D-MRI and OCT of the left eye (C, D1, D2): the norma basilaris; the white dashed line indicates the area of PS, the top of which is the point of optic nerve attachment. OCT shows the macula located on a slope. Both eyes are the same.

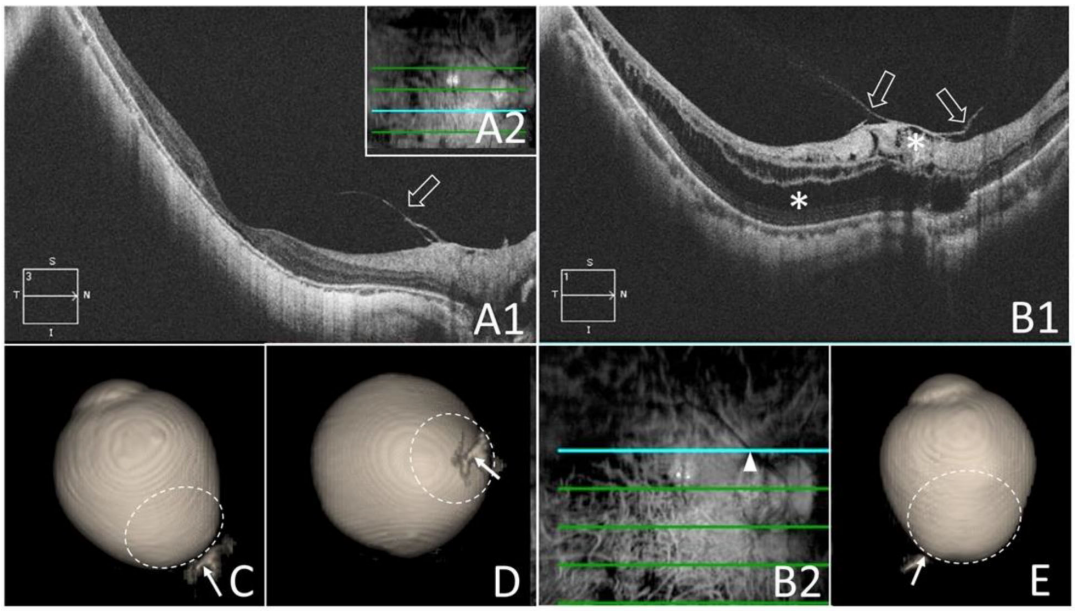

Figure 5. Binocular nasally distorted shaped eyes, nasal staphylomas. Binocular PM in a 28-year-old male patient whose SEs were −12 D/−12 D, BCVA values were 1.30 Log MAR/0.52 Log MAR, and ALs were 28.33 mm/29.69 mm in the right and left eyes, respectively. The *white arrow* in the figure indicates the optic nerve. OCT of the right eye (**A1**, **A2**): the *white hollow arrow* indicates vitreous traction. OCT of the right eye (**B1**, **B2**): another B-scan layer. The *white hollow arrow* indicates vitreous traction in the same place as the *white arrowhead* point and blood vessels. The *asterisks* show the inner and outer retinoschisis forming. The 3D-MRI of the right eye (**C**, **D**): the norma basilaris and norma occipitalis; the eye grows toward the nasal position, and the *white dashed line* indicates the PS, which is wide, indicating nasal staphyloma. The 3D-MRI of the left eye (**E**): the norma basilaris; the eye was barrel shaped, and the PS was of the narrow macular type, different from that in the right eye.

Results

General Information and Basic Characteristics

Fifty-nine patients (17 men and 42 women) and 108 eyes were included in this study. The average patient age was 48 ± 15 years. Of the 108 eyes, the SE was 17 D (approximately 12 to 20 D), the BCVA was 0.76 (approximately 0.33 to 1.28) Log MAR, and the average AL was 29.87 ± 2.07 mm. Ten monocular patients were included: two with single-eye atrophy, five with unilateral PM, and three requiring unilateral retinal reattachment operation. Forty-nine binocular patients were included.

The analysis of PS based on 3D-MRI revealed that 102 eyes of the 108 eyes that had PS, 55 (54.9%) had simple staphyloma, and 47 (46.08%) had complex staphyloma. Type I (Fig. 2) occurred in 56 eyes (52.5%), type II (Fig. 3) occurred in 27 eyes (26.7%), type III (Fig. 4) occurred in 8 eyes (5.0%), type IV (Figs. 5A–D) occurred in 1 eye (1.0%), type V (Fig. 6) occurred in 2 eyes (2.0%), and others (Fig. 7) occurred in 8 eyes (7.8%). The eye shape associated with type I was generally nasally distorted and barrel shaped ($\chi^2 = 8.417$; $P = 0.004$; Figs. 2C, 2D, 2E). The eye shape associated with type II was generally conical ($\chi^2 = 17.476$; $P < 0.05$; see Fig. 3). The eye shapes associated with type III and type IV were all nasally distorted (see Fig. 4; Figs. 5A–D). In this sample, 35 patients (71.4%) had the same eye shape in both eyes, and 37 patients (80.4%) had the same PS type.

OCT findings were observed in 81 of the 108 eyes: 10 eyes (12.4%) had a retinal hole (Fig. 2B1), 60 eyes (74.1%) had MRS (Fig. 2B1; Fig. 3B; Figs. 5A1, 5B1; Fig. 7B1; Figs. 8A1, 8B1), and 7 eyes (8.6%) had a dome-shaped macula (DSM; see Fig. 7).

Ocular Characteristics in Patients of Different Ages

We coded the right eye as 1 and left eye as 2 in 46 patients with binocular PS and used the random number extraction method to select one eye, adding 10 eyes from 10 monocular patients. The samples of 56 eyes in 56 people were analyzed.

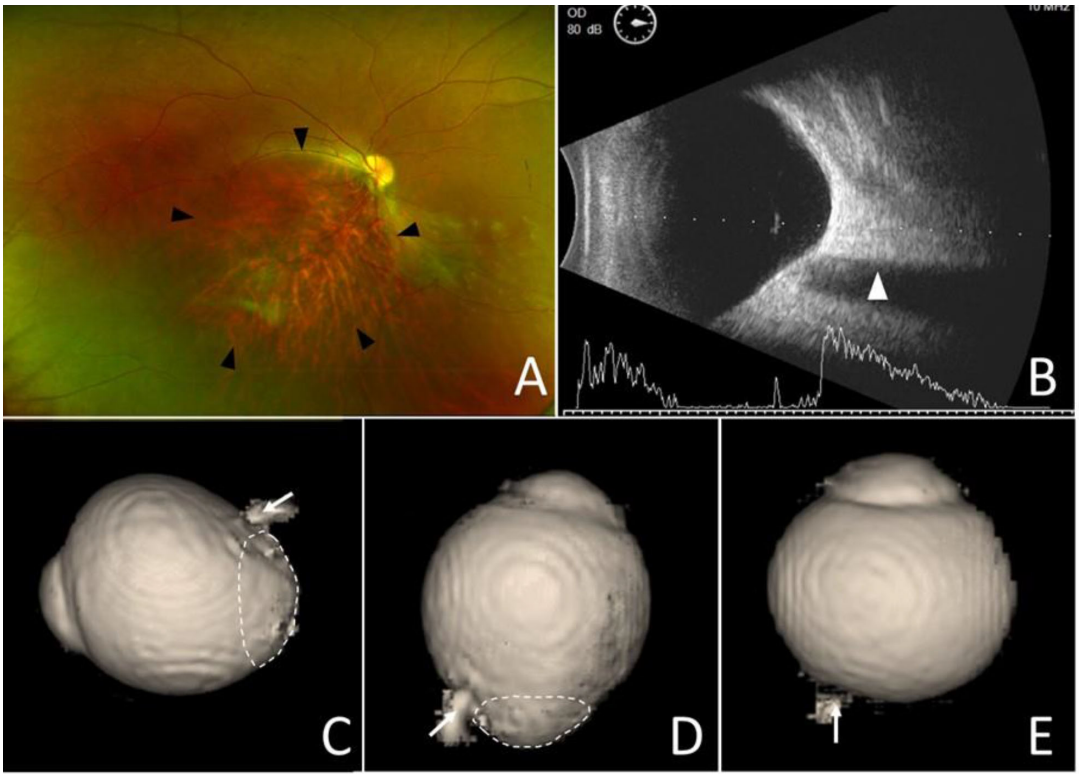

Figure 6. Monocular PM, conical-shaped right eye, inferior staphyloma in a 10-year-old male patient whose left eye showed emmetropia. The SE was −11 D, the BCVA was 1.30 Log MAR, and the AL was 26.82 mm in the right eye. The *white arrow* in the figure indicates the optic nerve. Fundus photograph of the right eye (**A**): the *black arrows* indicate the PS, which is located below the fundus, and the optic disc inclines toward the lower temporal position. B-Us of the right eye (**B**): the *white triangle* indicates the optic nerve, and the posterior of the eyeball is conical. The 3D-MRI of the right eye (C, D): the nasal view and norma superior. The temporal and nasal sides of the eyeball are symmetrical, and the eyeball is conical. The *white dashed line* indicates the PS, which is located below the point of optic nerve attachment, indicating inferior staphyloma. The 3D-MRI of the left eye (**E**): the norma basilaris; the eye shape was spheroidal.

Among the 56 eyes, the ages of patients who presented with simple type and complex type PS with normality after the Kolmogorov-Smirnov test were 43 ± 12 and 57 ± 12 years, respectively. The difference in the complexity of PS with patient age was statistically significant (F = 18.181; $P < 0.05$), with the complex type being more common in older patients.

AL, SE, and BCVA in Different PS Types

Of the 102 eyes with PS, the ALs of the eye with the simple type and complex type were 29.57 ± 2.40 mm and 30.52 ± 1.38 mm, respectively. The difference in the AL between simple PS and complex PS was statistically significant ($P = 0.003$), with longer ALs in complex PS. The ALs of eyes with type I and other types of PS were 30.47 ± 1.77 mm and 29.46 ± 2.11 mm, respectively. The difference in the AL between type I and other types of PS was statistically significant (F = 6.499, $P = 0.012$), with longer ALs in type I than the other types.

The SEs of eyes with the simple type and complex type were 15 D ± 5 D and 19 D ± 4 D, respectively. The difference in the SE between the simple type and the complex type was statistically significant (F =17.41, $P < 0.05$), with lower SEs in the complex type than the simple type. The difference in the SE between the different types of PS was not statistically significant ($P = 0.169$).

The BCVA values of the eyes with the simple type and complex type were 0.69 (approximately 0.22 to 1.00) Log MAR and 1.00 (approximately 0.69 to 1.20) Log MAR, respectively. The difference in the BCVA between the simple type and complex type was statistically significant ($P = 0.001$), with worse BCVA in the complex type than the simple type. The difference in the BCVA between the different types of PS was statistically significant ($P = 0.025$). The BCVA values of type I and other types of PS were 0.82 (approximately 0.52 to 1.30) Log MAR and 0.70 (approximately 0.22 to 1.00) LogMAR, respectively. The difference in the BCVA between type I and other types of PS was

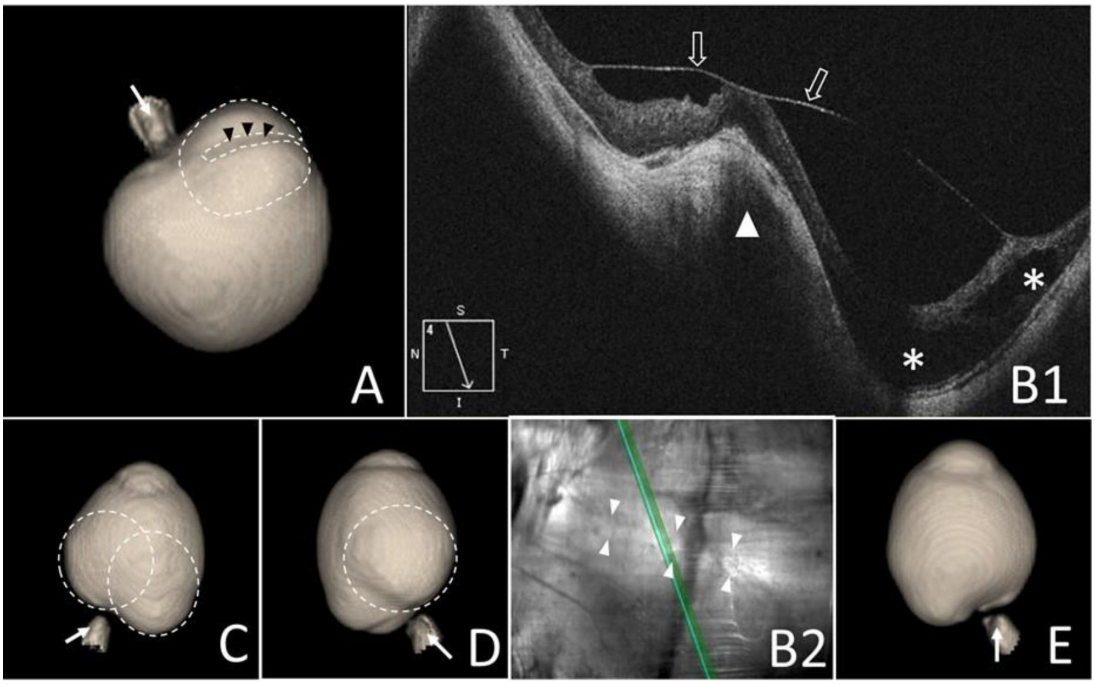

Figure 7. Binocular temporally distorted eyes, other staphylomas. Binocular PM in a 52-year-old female patient whose SEs were −23 D/−23 D, BCVA values were 1.00 Log MAR/1.30 Log MAR, and ALs were 28.26 mm/28.20 mm in the right and left eyes, respectively. The *white arrow* in the figure indicates the optic nerve. The 3D-MRI of the right eye (**C**, **D**): the norma basilaris and nasal view; two PS areas in different positions, with temporal distortions of the eye shape. OCT of the right eye (**B1**, **B2**): the *white hollow arrows* indicate proliferative membrane traction; the *asterisk* indicates the formation of inner and outer retinoschisis. The *white triangle* in **B1** shows the dome-shaped macula (DSM), corresponding to the area indicated by the *white arrowhead* in **B2** and the area indicated by the *black arrowheads* in (**A**). The 3D-MRI of the left eye (**E**): temporally distorted eyes; other staphylomas were the same as those in the right eye.

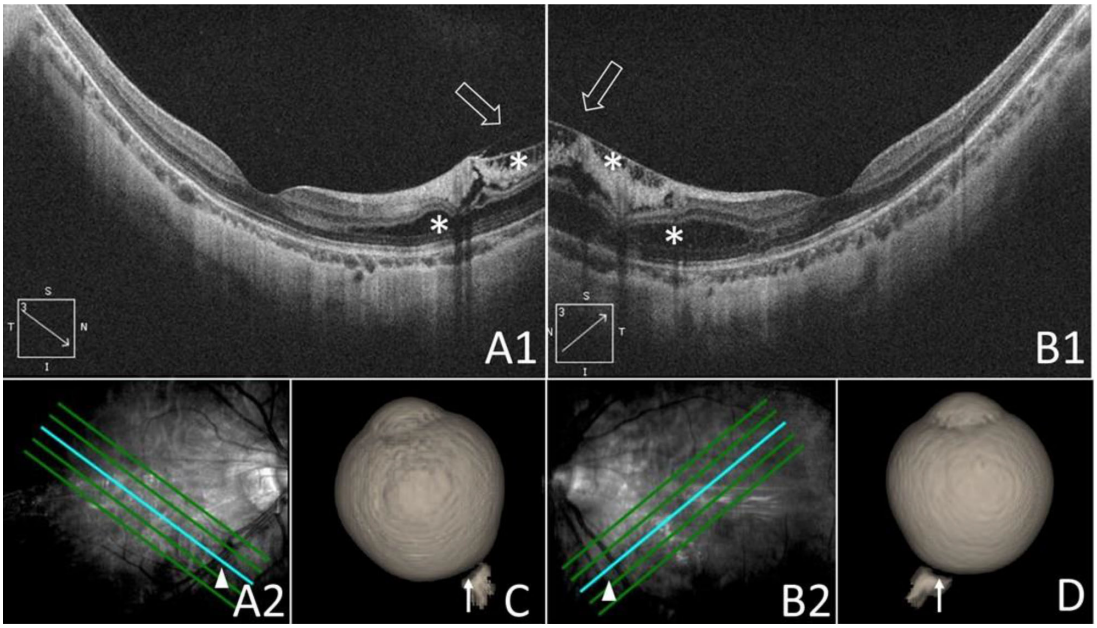

Figure 8. Binocular spheroidal shaped eyes, no staphyloma, mixed retinoschisis. Binocular PM in a 19-year-old male patient whose SEs were −10 D/−10 D, BCVA values were 0.00 LogMAR/0.05 LogMAR, and ALs were 29.19 mm/28.56 mm in the right and left eyes, respectively. The *white arrow* in the figure indicates the optic nerve. OCT of the right eye (**A1**, **A2**): the *white hollow arrow* indicates the vitreous traction; the *asterisk* indicates the formation of the inner and outer retinoschisis. The *white arrowhead* in **A2** indicates retinoschisis at the retinal vessels. The 3D-MRI of the right eye (**C**): the norma basilaris; the eyeball was spherically dilated, with no staphyloma. OCT and 3D-MRI of the left eye (**B1**, **B2**, **D**): same as that of the right eye.

statistically significant ($P = 0.049$), with worse BCVA in type I than the other types.

Relationship Between PS and MRS

We observed inner retinoschisis in 17 eyes (28.3%), outer retinoschisis (see Fig. 3B) in 15 eyes (25.0%) and mixed retinoschisis (see Figs. 5A1, 5B1; Fig. 7B1; Figs. 8A1, 8B1) in 28 eyes (46.6%) among the 60 eyes subjected to OCT. We also observed four eyes with mixed retinoschisis without PS (Fig. 8) in two young male patients. We observed 30 eyes (53.5%) with type I PS, 16 eyes (28.6%) with type II PS, 4 eyes (7.1%) with type III PS, 1 eye (1.8%) with type IV PS, 1 eye (1.8%) with type V, and 4 eyes (7.1%) with other PS. Most of the patients (93.3%) had MRS combined with PS, and the macular types (types I + II) were the most common (82.1%). The relationship between the type of MRS and wide macular ($\chi^2 = 0.509$, $P = 0.775$; Cramer's V = 0.095) or narrow macular ($\chi^2 = 1.670$, $P = 0.434$; Cramer's V = 0.173) PS was weak.

Discussion

We showed that eye shape and PS type were almost consistent in both eyes of patients, which is consistent with previous reports.[12,17] According to earlier reports,[20–22] the eye shape associated with PM and the type of PS changes with age. Patients with complex PS are usually older than those with simple PS, but the morphological changes in PS with age deserve further longitudinal studies. Previous studies[23–25] have suggested that the incidence of eye morphology changes increases with increasing age and AL and decreasing SE. In our study, patients with complex PS were older, and had a longer AL, a lower SE, and worse BCVA than those with simple PS, in accordance with previous studies.[26,27] Wide macular PS includes complex PS (Curtin's definition) in the latest classification definition.[28] In our study, macular PS (both wide and narrow macular PS) was the most common type at 79.2%, slightly lower than 88% and 79% in previous studies,[13,29] because our patients were younger than those in previous studies. Patients with wide macular staphyloma had a longer AL ($P = 0.012$) and worse BCVA ($P = 0.049$) than those with other types of PS. In our study, the rates of wide macular staphyloma, including complex PS and simple PS, were less than those in other studies. Based on our study and the results of previous studies,[22,30,31] we proposed that most of the eyes with PM initially present with a single narrow, macular and/or peripapillary staphyloma first; with age, multiple PSs fuse to form a wide, macular staphyloma, the AL continues to elongate, and the eye shape tends to achieve a barrel shape. Thus, eyes with PM are not only elongated but also unevenly expanded in the posterior sclera.[32]

Several studies[11,33] have suggested that AL elongation may cause mechanical damage to the retina and optic nerve by stretching the eyewall. In our study, MRS occurred with a high percentage in PS (93.3%), particularly in the macular type (82.1%). Moreover, we found that some eyes (12/60) had vitreous traction. However, among them, four eyes from two male patients presented with MRS, but not PS, a finding similar to the study findings of Sun et al.[34] Thus, MRS may also appear to be associated with vitreous traction, similar to the conclusions by Shinohara et al.[35] and Ikuno et al.[36] Thus, the occurrence of MRS is due to the combined action result of the vitreous-retinal interface and PS.[37] According to the theoretical causes of MRS, surgeons should consider the operation plan to treat MRS; the results of OCT and 3D-MRI are suggested to be analyzed, and PSR or pars plana vitrectomy (PPV) should be chosen cautiously to ensure that patients obtain admirable surgical benefits.

Because they change with age, PM, the shape of the eye, and PS are associated with visual prognosis; thus, these changes must be monitored. Our study showed that using 3D-MRI to observe eye shape and PS in PM had advantages. The 3D-MRI can indicate eye shape in vivo and in situ because it can comprehensively show the natural three-dimensional eye shape. The detection rate and accuracy of 3D-MRI are higher than those of B-mode ultrasound scans (B-US).[38] In the clinic, 3D-MRI allows convenient interpretation of the disease, guides clinical decisions, allows assessment of the prognosis, and assists in patient understanding of the disease. In studies, 3D-MRI simplifies PS classification, allowing the observance of morphological changes and comparison of the PS anatomy. Recent studies[35,39] have suggested that wide-field swept-source OCT could replace 3D-MRI, but it is not practical in large PS. However, 3D-MRI still has limitations. First, it is not suitable for patients with claustrophobia or mental issues and requires a high degree of patient cooperation. Second, MRI uses T_2-weighted images to reconstruct the intraocular fluid morphology; thus, it cannot show scleral morphology, the vitreous-retinal interface, or retinal interlayer changes. Additionally, the cost of this examination is high.

In this study, eye shape and PS type were based on the subjective judgment of the investigators. With the development of imaging technologies, future studies should focus on quantifying the curvature, size, and depth of PSs and clarifying the spatial points of a PS

in 3D image coordinates. For example, we should mark each point on a PS and know the spatial relationship to structures, such as the optic disc and fovea. This can provide dynamic biological modeling of PM.

Our study has limitations. First, the study included patients with PM referred to a large eye center. Therefore, the results may not represent the general population of PM individuals. Second, this study was a retrospective study with a small sample size, and only five individuals had undergone genotyping. Third, spectral domain-OCT did not allow the observation of morphological and pathological changes in the choroid and sclera.

Conclusions

Our results demonstrated that PS complexity increased with age and that PS was related to MRS. These changes were related to the visual acuity.

Acknowledgments

Funded by the National Natural Science Foundation of China (81770949), Henan Provincial of Department Science and Technology Project (162102410004), Zhengzhou Benefiting People Science and Technology Project (2019KJHM0002), Henan Eye Hospital Image and Artificial Intelligence Platform.

Author Contributions: G.A. and F.D. provided the conception and design. R.W., J.G., M.P., and Z.L. provided the data collection. G.A. provided the analysis and interpretation. X.J. and B. L. obtained funding. G.A., F.D., X.J., and B.L. provided overall responsibility of the study.

Disclosure: **G. An**, None; **F. Dai**, None; **R. Wang**, None; **J. Guo**, None; **M. Pan**, None; **Z.H. Lui**, None; **X. Jin**, None; **B. Lei**, None

* GA and FD made equal contributions to this study.

References

1. Cheng HC, Chang K, Shen E, Luo KS, Ying YH. Risk factors and behaviours of schoolchildren with myopia in Taiwan. *Int J Environ Res Public Health*. 2020;17(6):1967.
2. Wu JF, Bi HS, Wang SM, et al. Refractive error, visual acuity and causes of vision loss in children in Shandong, China. The Shandong Children Eye Study. *PLoS One*. 2013;8(12):e82763.
3. Choy BNK, You Q, Zhu MM, Lai JSM, Ng ALK, Wong IYH. Prevalence and associations of myopia in Hong Kong primary school students. *Jpn J Ophthalmol*. 2020;64(4):437–449.
4. Morgan IG, Ohno-Matsui K, Saw SM. Myopia. *Lancet*. 2012;379(9827):1739–1748.
5. Lim DH, Han J, Chung TY, Kang S, Yim HW, Epidemiologic Survey Committee of the Korean Ophthalmologic Society. The high prevalence of myopia in Korean children with influence of parental refractive errors: The 2008-2012 Korean National Health and Nutrition Examination Survey. *PLoS One*. 2018;13(11):e0207690.
6. Ohno-Matsui K, Lai TY, Lai CC, Cheung CM. Updates of pathologic myopia. *Prog Retin Eye Res*. 2016;52:156–187.
7. Naidoo KS, Fricke TR, Frick KD, et al. Potential lost productivity resulting from the global burden of myopia: systematic review, meta-analysis, and modeling. *Ophthalmology*. 2019;126(3):338–346.
8. Cooper J, Tkatchenko AV. A review of current concepts of the etiology and treatment of myopia. *Eye Contact Lens*. 2018;44(4):231–247.
9. Ohno-Matsui K, Kawasaki R, Jonas JB, et al. International photographic classification and grading system for myopic maculopathy. *Am J Ophthalmol*. 2015;159(5):877–83 e7.
10. Wong CW, Foo LL, Morjaria P, et al. Highlights from the 2019 International Myopia Summit on 'controversies in myopia'. *Br J Ophthalmol*, https://doi.org/1.1136/bjophthalmol-2020-316475. Online ahead of print.
11. Ohno-Matsui K, Jonas JB. Posterior staphyloma in pathologic myopia. *Prog Retin Eye Res*. 2019;70:99–109.
12. Guo X, Xiao O, Chen Y, et al. Three-dimensional eye shape, myopic maculopathy, and visual acuity: the Zhongshan Ophthalmic Center-Brien Holden Vision Institute High Myopia Cohort Study. *Ophthalmology*. 2017;124(5):679–687.
13. Ohno-Matsui K. Proposed classification of posterior staphylomas based on analyses of eye shape by three-dimensional magnetic resonance imaging and wide-field fundus imaging. *Ophthalmology*. 2014;121(9):1798–1809.
14. Gomez-Resa M, Bures-Jelstrup A, Mateo C. Myopic traction maculopathy. *Dev Ophthalmol*. 2014;54:204–212.

15. Gohil R, Sivaprasad S, Han LT, Mathew R, Kiousis G, Yang Y. Myopic foveoschisis: a clinical review. *Eye (Lond)*. 2015;29(5):593–601.
16. Wen B, Yang G, Cheng J, et al. Using high-resolution 3D magnetic resonance imaging to quantitatively analyze the shape of eyeballs with high myopia and provide assistance for posterior scleral reinforcement. *Ophthalmologica*. 2017;238(3):154–162.
17. Moriyama M, Ohno-Matsui K, Hayashi K, et al. Topographic analyses of shape of eyes with pathologic myopia by high-resolution three-dimensional magnetic resonance imaging. *Ophthalmology*. 2011;118(8):1626–1637.
18. Spaide RF. Staphyloma: Part 1. NewYork, NY: Springer, 2013:167–176.
19. Ceklic L, Munk MR, Wolf-Schnurrbusch U, Gekkieva M, Wolf S. Visual acuity outcomes of ranibizumab treatment in pathologic myopic eyes with macular retinoschisis and choroidal neovascularization. *Retina*. 2017;37(4):687–693.
20. Matsumura S, Kuo AN, Saw SM. An update of eye shape and myopia. *Eye Contact Lens*. 2019;45(5):279–285.
21. Pope JM, Verkicharla PK, Sepehrband F, Suheimat M, Schmid KL, Atchison DA. Three-dimensional MRI study of the relationship between eye dimensions, retinal shape and myopia. *Biomed Opt Express*. 2017;8(5):2386–2395.
22. Verkicharla PK, Ohno-Matsui K, Saw SM. Current and predicted demographics of high myopia and an update of its associated pathological changes. *Ophthalmic Physiol Opt*. 2015;35(5):465–475.
23. Wakazono T, Yamashiro K, Miyake M, et al. Time-course change in eye shape and development of staphyloma in highly myopic eyes. *Invest Ophthalmol Vis Sci*. 2018;59(13):5455–5461.
24. Chen M, Yu M, Dai J, Chu R. Long-term natural course of pathologic myopia in Chinese patients. *J Ophthalmol*. 2019;2019:1–6.
25. Saka N, Moriyama M, Shimada N, et al. Changes of axial length measured by IOL master during 2 years in eyes of adults with pathologic myopia. *Graefes Arch Clin Exp Ophthalmol*. 2013;251(2):495–499.
26. Hsiang HW, Ohno-Matsui K, Shimada N, et al. Clinical characteristics of posterior staphyloma in eyes with pathologic myopia. *Am J Ophthalmol*. 2008;146(1):102–110.
27. Chen Y, Xiao O, Guo X, et al. Methodology of the ZOC-BHVI High Myopia Cohort Study: the onset and progression of myopic pathologies and associated risk factors in highly myopic Chinese. *Ophthalmic Epidemiol*. 2018;25(1):31–38.
28. Ruiz-Medrano J, Montero JA, Flores-Moreno I, Arias L, Garcia-Layana A, Ruiz-Moreno JM. Myopic maculopathy: current status and proposal for a new classification and grading system (ATN). *Prog Retin Eye Res*. 2019;69:80–115.
29. Shinohara K, Shimada N, Moriyama M, et al. Posterior staphylomas in pathologic myopia imaged by widefield optical coherence tomography. *Invest Ophthalmol Vis Sci*. 2017;58(9):3750–3758.
30. Hayashi K, Ohno-Matsui K, Shimada N, et al. Long-term pattern of progression of myopic maculopathy: a natural history study. *Ophthalmology*. 2010;117(8):1595–1611, 1611 e1-4.
31. Chang L, Pan CW, Ohno-Matsui K, et al. Myopia-related fundus changes in Singapore adults with high myopia. *Am J Ophthalmol*. 2013;155(6):991–999 e1.
32. Jonas JB, Ohno-Matsui K, Panda-Jonas S. Myopia: anatomic changes and consequences for its etiology. *Asia Pac J Ophthalmol (Phila)*. 2019;8(5):355–359.
33. Takano M, Kishi S. Foveal retinoschisis and retinal detachment in severely myopic eyes with posterior staphyloma. *Am J Ophthalmol*. 1999;128(4):472–476.
34. Sun CB, You YS, Liu Z, et al. Myopic macular retinoschisis in teenagers: clinical characteristics and spectral domain optical coherence tomography findings. *Sci Rep*. 2016;6:27952.
35. Shinohara K, Tanaka N, Jonas JB, et al. Ultrawide-field OCT to investigate relationships between myopic macular retinoschisis and posterior staphyloma. *Ophthalmology*. 2018;125(10):1575–1586.
36. Ikuno Y, Gomi F, Tano Y. Potent retinal arteriolar traction as a possible cause of myopic foveoschisis. *Am J Ophthalmol*. 2005;139(3):462–467.
37. Wu PC, Chen YJ, Chen YH, et al. Factors associated with foveoschisis and foveal detachment without macular hole in high myopia. *Eye (Lond)*. 2009;23(2):356–361.
38. Shi J, He Y, Zhao T, et al. Reconstruct the high myopic eye modules with 3D—MRI imaging technology. *Chin J OptomOphthal Vis Sci*. 2016;18(5):269–274.
39. Ohno-Matsui K, Fang Y, Shinohara K, Takahashi H, Uramoto K, Yokoi T. Imaging of pathologic myopia. *Asia Pac J Ophthalmol (Phila)*, https://doi.org/1.22608/APO.2018494. Online ahead of print.